Modeling pattern formation and cavity solitons in quantum dot optical microresonators in absorbing and amplifying regimes

M. Brambilla, T. Maggipinto, and I. M. Perrini
CNR-INFM LIT3, Dipartimento Interateno di Fisica, Università e Politecnico di Bari, Via Orabona 4, 70126 Bari, Italy

S. Barbay and R. Kuszelewicz
Laboratoire de Photonique et de Nanostructures, LPN-CNRS, Route de Nozay, 91460 Marcoussis, France

(Received 2 March 2007; accepted 2 August 2007; published online 28 September 2007)

We present a complete overview of our investigation past and present of the modelization and study of the spatiotemporal dynamics of a coherent field emitted by a semiconductor microcavity based on self-assembled quantum dots. The modelistic approach is discussed in relation to prospective growth and experimental research, and the model is then applied to resonators for which the medium is either passive (coherent photogeneration of carriers) or active (carrier pumping by current bias). The optical response of the system is investigated, especially in what concerns the linewidth enhancement factor, which turns out to be critical for the onset of self-organized patterns. The regimes in which one can expect bistable response, modulational instabilities, pattern formation, and cavity soliton formation are investigated. The pattern scenario is described, and experimentally achievable conditions are predicted for the occurrence of stable cavity solitons. © *2007 American Institute of Physics*. [DOI: 10.1063/1.2775414]

The analysis of unstable and chaotic phenomena has found fertile ground in the field of nonlinear optics, and within the framework of the extensive literature on optical pattern formation, the recent studies concerning cavity solitons (CS) seem to indicate an interesting avenue in the direction of optical information processing. The standard configuration is that of an optical cavity containing a nonlinear medium and driven by a stationary holding beam that provides energy to the system. CS are localized intensity peaks that appear in a homogeneous background of radiation. They do not diffract, and can be manipulated as single entities. From the practical viewpoint of miniaturization and fast time scales, the case in which the optical nonlinear medium is a semiconductor is extremely interesting. Semiconductor microcavities containing a multiple quantum well or a bulk medium have already been analyzed. In this paper, we consider the case of a quantum dot (QD) semiconductor by developing a model that takes into account the features of QD optical response most relevant to the spatiotemporal dynamics of the coherent field. We study those features with the aim to compare them to more complex "first-principles" models and to provide a guideline for sample development and experiments in progress.

I. INTRODUCTION

The prediction[1] and experimental confirmations of addressable cavity solitons (CS) in broad-area semiconductor microresonators[2–5] have opened up the perspective of exploiting self-confined, self-organized structures in the coherent field as a means to realize new optoelectronic devices for all-optical information encoding, routing, buffering, delaying, and commutation. The interest resides not only in such appealing applications, but also in the achievement of stable CS in systems exhibiting a rich scenario of spontaneous pattern formation and localization in the simplest layouts, designs, and growth requirements. Recent work has addressed these issues, suggesting the use of microlasers with an injected signal[6] or VECSELs with saturable absorbers where no coherent injection is required to sustain the pattern formation process and where CS are emitted directly above the lasing threshold.[7]

At the same time, optical devices based on an InGaAs multiple-quantum-dot active medium have attracted considerable attention for their promising properties, such as low threshold, fast dynamics, large bandwidth, lack of filamentation at high bias (Ref. 8 and references therein), and for interesting nonlinear dynamic effects experimentally observed in devices with peculiar characteristics.[9,10]

From a more fundamental viewpoint, the use of a collection of QD as a nonlinear medium in a microcavity offers the opportunity to access the typical nonlinear response of quasi-two-level atoms, with reduced diffusive effects, the possibility of a fast carrier dynamics and high saturation intensities, and in particular the accessibility of a self-focusing nonlinearity when the QD resonances lie far from the continuum contributions of the susceptivity [e.g., from the wetting layer (WL)].

In fact, QD are the sole solid-state heterostructures to possess a discrete energy spectrum of bound states. Therefore, in terms of optical transitions, QD behave much like atoms and they provide access to the high-energy side of their electronic transitions at excitation regimes below transparency. For example, in the purely dispersive case, the sign of the nonlinear effect influences the observation of temporal or spatial solitons,[11,12] while a self-focusing nonlinearity was

shown to be more favorable for the existence of the so-called cavity solitons.[13]

However, the comparison between QD and atoms cannot be pushed too far, essentially because in solids, quantum confinement is obtained as an overmodulation of a crystal potential. As a result, the confinement properties still coexist with the collective electronic properties. For example, one of the most common techniques for realizing self-assembled QD is to use the Stransky-Krastanov growth regime where the QD sit on an ultrathin two-dimensional (2D) quantum well of a few atomic monolayers thickness called the wetting layer. This introduces a coupling mechanism between the set of discrete energy levels of the QD and the WL continuum of states that sensibly modifies the light-matter interaction as compared to the atomic model.

Furthermore, in our model, pumping may be provided to obtain optical gain in a QD system, and the injection, be it an incoherent optical excitation or an electric bias current, occurs into the WL, so that the gain in the medium, where the resonant interaction with the coherent field occurs, depends on the coupling mechanisms. In fact, the complete understanding of the optical properties, and the modelization thereof, in QD lasers is presently a focus of debate and interest, and the treatment is far from elementary.[14]

Our research focuses on the effects of the QD susceptivity with respect to the spatiotemporal dynamics of the 2D field inside the broad-area cavity, analyzing the onset of modulational instabilities, which lead to spontaneous pattern formation and to the prediction of stable CS in a MQD-based vertical microresonator driven by a coherent external field; a pumping mechanism in the WL may or may not be considered, i.e., we analyzed both the "active" and "passive" configurations.

The scope of the present paper is not to provide a detailed and original modeling of the response of QD on a microscopic scale;[15–17] we would rather consider those basic mechanisms that describe the QD response without pushing the model complexity too far, concentrating the physical insight on the pattern-forming mechanisms. So the aim of the paper is to provide a guideline for sample growth and experimental operational regimes in which CS might be found in forthcoming experiments.

In this paper, we will provide an overview of our modelization of the above-mentioned system starting from the simplest approach consisting in modeling a collection of inhomogeneously broadened two-level resonances,[18] and moving on to the inclusion of WL-QD coupling mechanisms.[19] An original contribution will be presented here for the description of pumped (active) devices, where we will consider the gain, dispersion, and alpha factor of a microlaser in the amplifying regime. We will also complement previous results described elsewhere in the passive devices, with new evidence concerning the role of capture and escape rates depending on the energy distribution of the QD collection. Our results show encouraging qualitative (and at times quantitative) agreement with previous works, more devoted to the study of QD lasers, including the prediction of regimes where negative alpha (linewidth enhancement or Henry) factors can be predicted.[20,21] Of course our approach is limited to the general regimes in which the quest for stable CS has been more successful, and thus we will not cover highly saturated regimes and/or strong pumping as in Ref. 22, where the plasma contributions seem to be quite relevant for the determination of the alpha factor. Also, we will model samples with shallow QD, well isolated from the WL levels. The section devoted to the model description will state and discuss the span of our approach. We next investigate both the passive and the active regimes.

The last part of this paper will provide some nonexhaustive analysis of the parameter space, which is meant to provide indications for the QD densities and the possible number of stacked QD layers, necessary to search for self-organization in the coherent field, but also to determine the pumping level and the conditions for the coherent injected field.

II. THE MODEL

The model presented here is based on the one we developed in Refs. 18 and 19, which we recall for the sake of completeness. We consider a broad-area vertical-cavity microresonator of the Fabry-Perot type, driven by an external coherent beam at room temperature. The light-matter interaction takes place in the active medium, which consists of a layer of QD perpendicular to the propagation direction z of the radiation inside the cavity.

QD are quasi-zero-dimensional systems where electrons and holes are confined in the three spatial dimensions. Therefore, all their bound states are discrete levels. Energy levels are highly dependent on the QD geometry, the strain between the dot and the host material, and on the material involved. Therefore, some general assumptions on the electronic structure of the QD are necessary in order to build a suitable model.

The simplest approach consists of neglecting all the possible interactions between the dots itself and the WL on which they sit and taking into account a key property of QD that results from the fluctuation of the dot size and leads to a correlated fluctuation of the transition energy. This fluctuation is isotropic in the transverse plane and yields a spatially uniform inhomogeneous broadening of the resonance characterized by a linewidth Γ and a central frequency ω_a^C.

To account for this, following a path already described in Refs. 18 and 19, we weigh the contribution of each class of dots by a Gaussian statistical weight,

$$G(\Delta_i,\Delta)=\frac{1}{(\Gamma/\gamma_P)\sqrt{\pi}}\exp\left[-\left(\Delta_i-\frac{\gamma_P}{\Gamma}\Delta\right)^2\right], \tag{1}$$

where $\Delta_i=(\omega_a^C-\omega_0)/\Gamma$ is the normalized field detuning from the QD population line center. The susceptibility of the inhomogeneously broadened QD population then stems from the summation of the responses of individual QD weighted by their Gaussian statistical contribution. The dynamics of this prototypal model is described by the equation for the field inside the cavity and of the quantum dot carrier density and basically resembles the scheme already found for the MQW model. However, the lack of any kind of interaction

between QD and WL is a strong limitation that also inhibits the possibility of considering active regimes.

As a refinement, we thus consider here the QD fundamental transition coupled to the WL. The coupling and relaxation mechanisms are complex and not fully understood yet, and so we shall incorporate them in our model through phenomenological escape and capture transition rates. The coupling mechanism between the WL and the QD is twofold. On the one hand, carriers can escape or can be captured by the dot via thermo-activation through emission or absorption of lattice phonons. On the other hand, Auger processes can also participate in the carrier exchange between the WL and the QD.

In what follows, we consider the quantum dot occupation number for the electrons and holes $n^{e,h}$, given by the sum over opposite spins of the single-particle states. Since in our model we take into account only the fundamental QD transition, the level degeneracy is $\Pi=2$ for the two opposite spins. In addition, we neglect the transition energy difference for the exciton and the biexciton states since it is usually very small compared to other broadening mechanisms that will be introduced in the following. In the rotating wave approximation and taking the dipole matrix element d as real, the equations for the dot population and the total polarization P_{QD} can be written as follows:[19]

$$\frac{dn^{e,h}}{dt} = -\gamma_{\mathrm{nr}} n^{e,h} - \Gamma_{\mathrm{sp}} n^e n^h + \frac{id}{\hbar}(EP^*_{\mathrm{QD}} - E^* P_{\mathrm{QD}}) + \left.\frac{\partial n^{e,h}}{\partial t}\right|_{\mathrm{QD\text{-}WL}} + \left.\frac{\partial n^{e,h}}{\partial t}\right|^{\mathrm{Auger}}_{\mathrm{QD\text{-}WL}}, \tag{2}$$

$$\frac{dP_{\mathrm{QD}}}{dt} = -\gamma_p(i\Delta + 1)P_{\mathrm{QD}} - \frac{idE}{\hbar}(n^e + n^h - \Pi), \tag{3}$$

where γ_{nr} and Γ_{sp} are the nonradiative and spontaneous recombination rate, respectively, E is the electric field envelope with pulsation ω_0, d is the real dipole matrix element, γ_p is the half-width of the electron-hole state, and $\Delta = (\omega_a - \omega_0)/\gamma_p$ is the normalized single dot detuning from resonance, ω_a being the central electron-hole transition frequency.

In the equation for the carrier population, the first QD-WL relaxation term refers to the thermoactivated processes as described before,

$$\left.\frac{\partial n^{e,h}}{\partial t}\right| = -\gamma^{e,h}_{\mathrm{esc}} n^{e,h} + \sigma^{e,h}_{\mathrm{cap}} N^{e,h}_{\mathrm{WL}}(\Pi - n^{e,h}), \tag{4}$$

where $N^{e,h}_{\mathrm{WL}}$ is the surface density carrier population in the WL. $\gamma^{e,h}_{\mathrm{esc}}$ and $\sigma^{e,h}_{\mathrm{cap}}$ are, respectively, the escape rate from the QD and the capture rate cross section into the QD. Contrary to Ref. 19, here we improve the modeling by considering the escape rates not as constants, but dependent on the normalized single dot detuning from resonance and from the normalized detuning from the central line distribution. In order to show this, let us suppose that carriers can thermally escape in a time τ^{ES} from the excited state (ES) (the electron-hole pair) into the WL. The escape time can be derived by assuming that the system reaches a quasi-Fermi equilibrium in the absence of external excitation and hence it can be written as[23,24]

$$\tau^{\mathrm{ES}} \propto \exp\left(\frac{E_{\mathrm{WL}} - E_{\mathrm{ES}}}{k_B T}\right). \tag{5}$$

The direct physical interpretation is that when the difference in energy between the WL and the ES is bigger, the carrier lasts long in the excited state, i.e., it is more difficult for it to escape into the WL. γ_{esc} is just the inverse of the escape time and hence its dependence is proportional to $\exp[(E_{\mathrm{ES}} - E_{\mathrm{WL}})/k_B T]$.

After some algebra, we obtain

$$\begin{aligned}\gamma_{\mathrm{esc}} &\propto \exp\left(\frac{\hbar\gamma_p\Delta + \hbar\omega_0 - E_{\mathrm{WL}}}{k_B T}\right) \\ &= \exp\left(\frac{\hbar\omega_0 - E_{\mathrm{WL}}}{k_B T}\right)\exp\left(\frac{\hbar\gamma_p}{k_B T}\Delta\right) \\ &= \mathrm{const}\cdot\exp\left(-\frac{\Gamma}{\gamma_p}\beta\Delta_i\right)\exp(\beta\Delta),\end{aligned} \tag{6}$$

where $\beta = \hbar\gamma_p/k_B T$. For typical parameters at room temperature, β is of the order of 0.01/0.02. As for σ_{cap}, the situation is quite the opposite in the sense that the transition from the WL into the excited state is favored when the difference $E_{\mathrm{WL}} - E_{\mathrm{ES}}$ is bigger, i.e., the opposite situation as described above and hence the final result is that $\sigma_{\mathrm{cap}} \propto \exp[(\Gamma/\gamma)\beta\Delta_i]\exp(-\beta\Delta)$.

In their final form, the capture and escape coefficient can be taken as

$$\gamma_{\mathrm{esc}} = \bar{\gamma}_{\mathrm{esc}}\cdot\exp\left(-\frac{\Gamma}{\gamma_p}\beta\Delta_i\right)\exp(\beta\Delta), \tag{7}$$

$$\sigma_{\mathrm{cap}} = \bar{\sigma}_{\mathrm{cap}}\exp\left(\frac{\Gamma}{\gamma}\beta\Delta_i\right)\exp(-\beta\Delta). \tag{8}$$

The second QD-WL relaxation term in Eq. (2) describes the Auger processes; the Auger dynamics of the electrons can be cast as follows:[19]

$$\left.\frac{\partial n^e}{\partial t}\right|^{\mathrm{Auger}}_{\mathrm{QD\text{-}WL}} = -B_{he}N^h_{\mathrm{WL}}n^e(\Pi - n^h) + B_{eh}N^e_{\mathrm{WL}}n^h(\Pi - n^e), \tag{9}$$

where we have retained only terms at first order in $N^{e,h}_{\mathrm{WL}}$, as their contribution is the highest. The first term describes the excitation of an electron to the WL via the interaction of a hole in the WL and in the QD, and the second term describes the capture of a WL electron in the QD via the interaction of a WL and a QD hole. Note that the two processes, characterized by the two cross-sectional rates B_{he} and B_{eh}, are clearly symmetric.

A similar term exists for the holes,

$$\left.\frac{\partial n^h}{\partial t}\right|^{\mathrm{Auger}}_{\mathrm{QD\text{-}WL}} = \left.\frac{\partial n^e}{\partial t}\right|^{\mathrm{Auger}}_{\mathrm{QD\text{-}WL}}. \tag{10}$$

Given the fast polarization decay time for the QD polarization γ_p^{-1} with respect to other decay times, we can perform and adiabatic elimination of P_{QD} in Eq. (3).

The rate equation for the WL carrier population is given by

$$\frac{\partial N_{\mathrm{WL}}^{e,h}}{\partial t} = \Lambda - \gamma_{\mathrm{nr}}^{\mathrm{WL}} N_{\mathrm{WL}}^{e,h} + \left.\frac{\partial N_{\mathrm{WL}}^{e,h}}{\partial t}\right|_{\mathrm{QD\text{-}WL}} + \left.\frac{\partial N_{\mathrm{WL}}^{e,h}}{\partial t}\right|_{\mathrm{QD\text{-}WL}}^{\mathrm{Auger}} + D\nabla_{\perp}^2 N_{\mathrm{WL}}^{e,h}, \tag{11}$$

where Λ represents the current pumping carriers in the WL, and $\gamma_{\mathrm{nr}}^{\mathrm{WL}}$ represents the nonradiative decay (radiative decays are neglected since they are second order in N_{WL}).

In contrast with Ref. 19, here we will study also the active regime and hence we will consider the effect of the pumping term on the final results.

The diffusion coefficient D accounts for a diffusive coupling of QD at different locations. Considering a constant spatial density of QD(N_{QD}), the Auger term and the capture term read

$$\left.\frac{\partial N_{\mathrm{WL}}^{e,h}}{\partial t}\right|_{\mathrm{QD\text{-}WL}}^{\mathrm{Auger}} = -N_{\mathrm{QD}} \left.\frac{\partial n^{e,h}}{\partial t}\right|_{\mathrm{QD\text{-}WL}}^{\mathrm{Auger}} \quad \text{and}$$
$$\left.\frac{\partial N_{\mathrm{WL}}^{e,h}}{\partial t}\right|_{\mathrm{QD\text{-}WL}} = -N_{\mathrm{QD}} \left.\frac{\partial n^{e,h}}{\partial t}\right|_{\mathrm{QD\text{-}WL}}. \tag{12}$$

After proper rescaling, as described, for example, in Ref. 19, the rate equation for electrons and holes and for the WL can be recast in the following adimensional form:

$$\frac{\partial n^{e,h}}{\partial t} = -\gamma\left(n^{e,h} + \frac{\Gamma_{\mathrm{sp}}}{2} n^e n^h + \frac{|E|^2}{1+\Delta^2}(n^e + n^h - \Pi) \pm B_{he} N_{\mathrm{WL}}^h n^e (\Pi - n^h) \mp B_{eh} N_{\mathrm{WL}}^e n^h (\Pi - n^e) + \gamma_{\mathrm{esc}}^{e,h} n^{e,h} - \sigma_{\mathrm{cap}}^{e,h} N_{\mathrm{WL}}^{e,h} (\Pi - n^{e,h})\right), \tag{13}$$

$$\frac{\partial N_{\mathrm{WL}}^{e,h}}{\partial t} = -\gamma^{\mathrm{WL}}\left(-\Lambda + N_{\mathrm{WL}}^{e,h} - D\nabla_{\perp}^2 N_{\mathrm{WL}}^{e,h} \mp B_{he} N_{\mathrm{WL}}^h \int n^e (\Pi - n^h) G(\Delta_i, \Delta) d\Delta \pm B_{eh} N_{\mathrm{WL}}^e \int n^h (\Pi - n^e) G(\Delta_i, \Delta) d\Delta - \gamma_{\mathrm{esc}}^{e,h} \int n^{e,h} G(\Delta_i, \Delta) d\Delta - \sigma_{\mathrm{cap}}^{e,h} N_{\mathrm{WL}}^{e,h} \int (\Pi - n^{e,h}) G(\Delta_i, \Delta) d\Delta\right). \tag{14}$$

As for the equation for the intracavity electric field, it is obtained by following the usual procedure described, e.g., in Refs. 13 and 25. In the slowly varying envelope approximation and in the mean-field limit, we can cast the equation in the following adimensional form:

$$\frac{\partial E}{\partial t} = -\left[(1 + i\vartheta)E - E_I - i\nabla_{\perp}^2 E - 2C\left(\int \frac{1 - i\Delta}{1 + \Delta^2}(n^e + n^h - \Pi) G(\Delta_i, \Delta) d\Delta\right) E\right], \tag{15}$$

where $\vartheta = (\omega_c - \omega_0)/\kappa$ is the scaled cavity field detuning, with $\kappa = cT/2n_b L$ the field decay rate, where, as usual, c is the speed of light in vacuum, T is the transmissivity of the mirror, n_b is the background refractive index, and L is the cavity length. C is the bistability parameter accounting for the coupling strength between the field and the active material and is directly linked to the spatial density of QD being defined as $2C = (d^2 \omega_0 N_{\mathrm{QD}})/(\varepsilon_0 \hbar \gamma_p n_b c T)$, E_I refers to the field injected into the cavity, and the transverse Laplacian $\nabla_{\perp}^2$ accounts for the diffraction in the transverse plane. The time coordinate is scaled to the field decay time κ^{-1} while the spatial transverse coordinates are rescaled to the square root of the diffraction length $a = c/2n_b k_0 \kappa$, where k_0 is the field wave vector.

III. PASSIVE REGIME

The passive regime has already been investigated in detail in Ref. 19, and we recall here the main results obtained there. First of all, we have checked that in the passive configuration, i.e., when the sole injected beam provides a pure optical generation of carriers, by neglecting the QD-WL interactions, it is possible to reduce the complete model to the simple two-level inhomogeneously broadened model,[18] thus assessing the consistency of our approach.

Reintroducing the QD-WL interactions, we have evaluated the role of the various terms. We have found that the steady-state values of the field and the electron and hole densities do not depend to a great extent on the Auger effect and radiative recombination. On the contrary, the stationary curves and the domains of modulational instability (MI), i.e., instabilities against a modulated perturbation, are more significantly influenced by the QD-WL relaxation mechanisms ($\gamma_{\mathrm{esc}}^{e,h}$ and $\sigma_{\mathrm{cap}}^{e,h}$). As already mentioned in the preceding section, and contrary to Ref. 19, the capture and escape terms in the present model depend on the QD transition energies and on the single dot family detuning; we will show how these new dependencies influence the results obtained in Ref. 19.

We have studied three physical situations corresponding to a good carrier confinement inside the QD($\bar{\gamma}_{\mathrm{esc}}^e = \bar{\gamma}_{\mathrm{esc}}^h = 0.01$), a poor one ($\bar{\gamma}_{\mathrm{esc}}^e = \bar{\gamma}_{\mathrm{esc}}^h = 100$), and an intermediate situation where the hole confinement is weaker than that of the electrons,($\bar{\gamma}_{\mathrm{esc}}^h = 100$, $\bar{\gamma}_{\mathrm{esc}}^e = 0.01$); these regimes have been analyzed in terms of the corresponding plane-wave instabilities (PWI), i.e., instabilities against a plane homogeneous perturbation, and MI. At the end, in order to appreciate the new features that emerge when considering QD-WL interactions, we have considered the intermediate confinement case. This choice has been adopted both for the focusing ($\Delta_i = -1$) and defocusing ($\Delta_i = 0.5$). As for the value of other parameters, we have tried to keep as close as possible to the regimes studied in Ref. 18 while compromising for the most promising indications for stable solitonic branches, and thus we have considered, as in Ref. 19, the following choices of

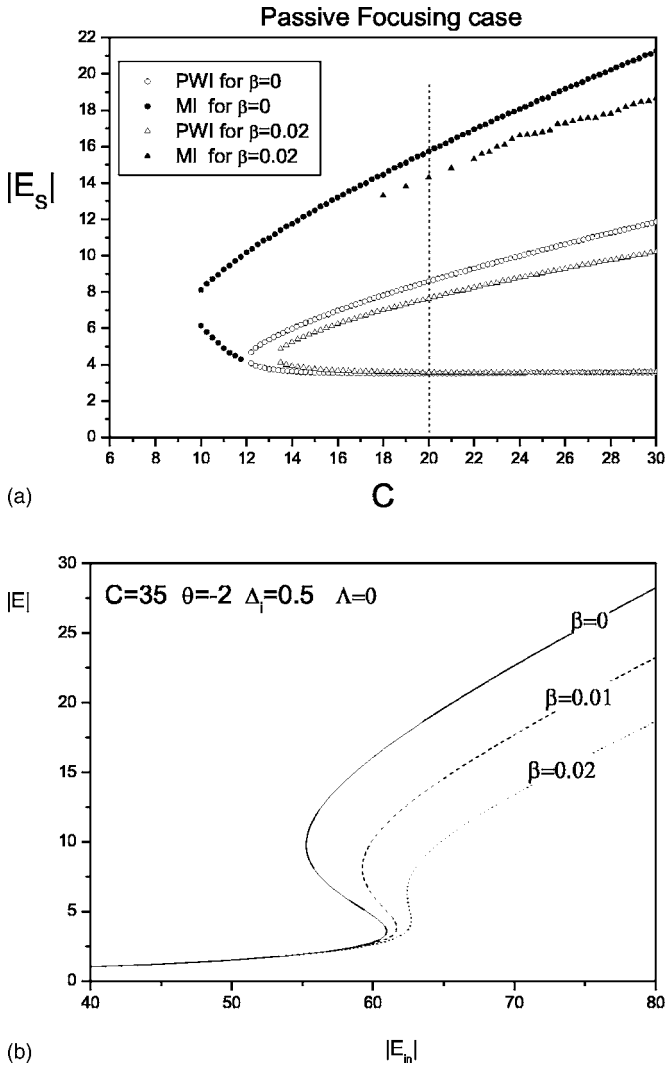

FIG. 1. (a) PWI and MI boundaries vs C for the focusing set of parameters. The vertical line corresponds to the specific value of C that is chosen for the pattern-formation analysis; (b) steady-state homogeneous curves for the defocusing case for three different values of β.

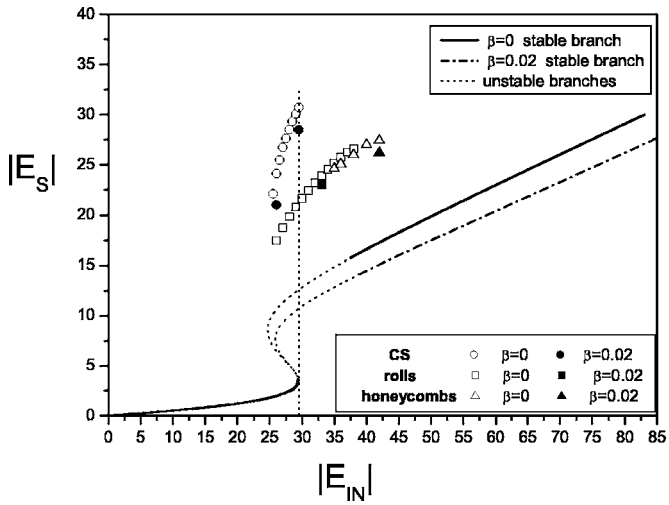

FIG. 2. Passive focusing regime. Steady-state curves of the homogeneous solutions for $\beta=0$ and 0.02. Complete pattern characterization is for $\beta=0$, and for comparison only, some checkpoints for pattern characterization are for $\beta=0.02$. The ordinate corresponds to the maximum intracavity field amplitude in the patterns.

parameters: $\bar{\sigma}_{\mathrm{cap}}=500$, $\gamma=15$, $\Gamma=60$, $B_{he,eh}=500$, $\Gamma_{\mathrm{sp}}=2.5$, $D=0.41$, and $\theta=-3$ for the focusing case, and $\theta=-2$ for the defocusing one. As for the choice of the value of C, we have studied the steady-state curves searching for PWI and MI. We recall that the search for PWI consists in finding the region of negative slope in the homogeneous steady-state curve, and a bistable behavior is highly desirable when searching for CS branches. The guiding criterion for choosing C is that we should have a well-defined bistability and a good portion of MI on the upper homogeneous branch.

In Fig. 1(a), we plot the values of the intracavity steady-state homogeneous field $|E_S|$ corresponding to MI and PWI boundaries for different values of C in the focusing regime. Together with the old results also reported in Ref. 19, here we superimpose/compare the new results obtained when capture and escape terms depend on detuning. An interesting and original result is that for $\beta=0.02$ the boundaries for MI and PWI are slightly affected and thus we can continue to adopt for C the values chosen in,[19] i.e., $C=20$. As for the defocusing case, we have checked that the introduction of the energy dependency in $\gamma_{\mathrm{esc}}^{e,h}$ and $\sigma_{\mathrm{cap}}^{e,h}$ affects to a greater extent the PWI and MI boundaries; this is shown, for example, in Fig. 1(b), where we plot the steady-state homogeneous curve for $C=35$ and for $\beta=0/0.01/0.02$. We see that by increasing the value of beta, the curve gradually loses the bistable character. This, however, is not detrimental for our purposes since we are more interested to the self-focusing regime, which is known to favor the formation of CS and which is easily accessible in a QD microcavity.

We thus report in Fig. 2 the old results obtained with $\beta=0$, together with the new results for $\beta=0.02$. We have performed a few, sampled, numerical simulations that confirmed a very similar pattern zoology. As an example, for $\beta=0.02$ we superimpose the starting and the final points of the CS branch (indicated by filled circles) and only two more sample points representing the roll and the honeycomb patterns. We can see that honeycomb patterns are met subcritically beyond the onset of MI on the upper branch of the homogeneous curve. Decreasing the input field, the honeycombs destabilize in favor of roll patterns that eventually evolve in a cluster of CS. Stable CS are found by means of the usual addressing technique described, e.g., in Ref. 13. Stable CS are found from $|E_{\mathrm{in}}|=25.5$ for $\beta=0$ and from $|E_{\mathrm{in}}|=26$ for $\beta=0.02$ up to the value of the input field corresponding to the lower homogeneous branch turning point, and this also confirms that CS need a stable homogeneous branch upon which to sit.

As for the defocusing regime, we find a similar scenario for the pattern zoology, and in contrast to what is usually observed,[13] it does not seem to be less favorable than the focusing one to the occurrence of CS, at least for our parameter choice. The only difference from the focusing case is that, when considering energy-dependent escape and capture terms, in order to obtain similar PWI and MI boundaries as in Ref. 19, we should take higher values of C and this in turn reflects on the density of QD as described in the section devoted to the model.

IV. ACTIVE REGIME

A. Transparency and lasing

One of the first issues in studying the pumped case has been the determination of the transparency and lasing thresholds in order to work between the two. To this end, we first note that the susceptibility describing the matter field interaction can be cast as

$$\chi = -\int \frac{\Delta + i}{1+\Delta^2}(n^e + n^h - \Pi)G(\Delta_i,\Delta)d\Delta, \tag{16}$$

thus being

$$\mathrm{Re}(\chi) = -\int \frac{\Delta}{1+\Delta^2}(n^e + n^h - \Pi)G(\Delta_i,\Delta)d\Delta,$$

$$\mathrm{Im}(\chi) = -\int \frac{1}{1+\Delta^2}(n^e + n^h - \Pi)G(\Delta_i,\Delta)d\Delta.$$

As usual, the absorption/gain behavior is linked to positive/negative sign of the imaginary part of the susceptibility and hence the transparency threshold is met when a change of sign does occur. A series of numerical simulations have shown that the transparency value of the pump turns out to be independent of the parameters C, ϑ, and Δ_i in a fashion similar to the obvious independence in the MQW case. On the other hand, the transparency value depends on the capture and escape rate coefficients σ_{cap} and γ_{esc}. Then once we introduce the asymmetry due to the dependence from Δ and Δ_i in these rates, we expect that transparency depends on Δ_i.

The free lasing threshold is determined as the pump Λ value at which the intracavity field starts growing in the absence of an injected field. In Fig. 3(a) we plot the lasing and the transparency thresholds when varying C for a fixed value of Δ_i, while in Fig. 3(b) the same thresholds are reported versus Δ_i while keeping C fixed. The lasing threshold depends as expected on the coupling parameter C and on the detuning from the central-line distribution. By decreasing the coupling parameter or by increasing the detuning from the central-line distribution, the value of the lasing threshold becomes too high and difficult to obtain in an experimental setup, e.g., in Fig. 3(a) we see that at $C=15$ the pump value should be $\Lambda=32$. Such high values of the pump would determine an extreme WL population not reachable in the current state-of-the-art molecular beam epitaxy.

For what concerns the numerical values of the various parameters entering into the model, the choice has been steered by preliminary experimental indications and will be explained later on; they are reported in the caption. As for the β factor, in these numerical simulations it is kept fix at $\beta=0.02$.

B. Linewidth enhancement factor for QD

An important parameter is the linewidth enhancement factor, which quantifies the degree to which variations in the carrier density alter the index of refraction at a certain wavelength and which is given by $\alpha \propto (dn/dN)/(dg/dN)$, where n is the refractive index, g is the gain per unit length, and N is

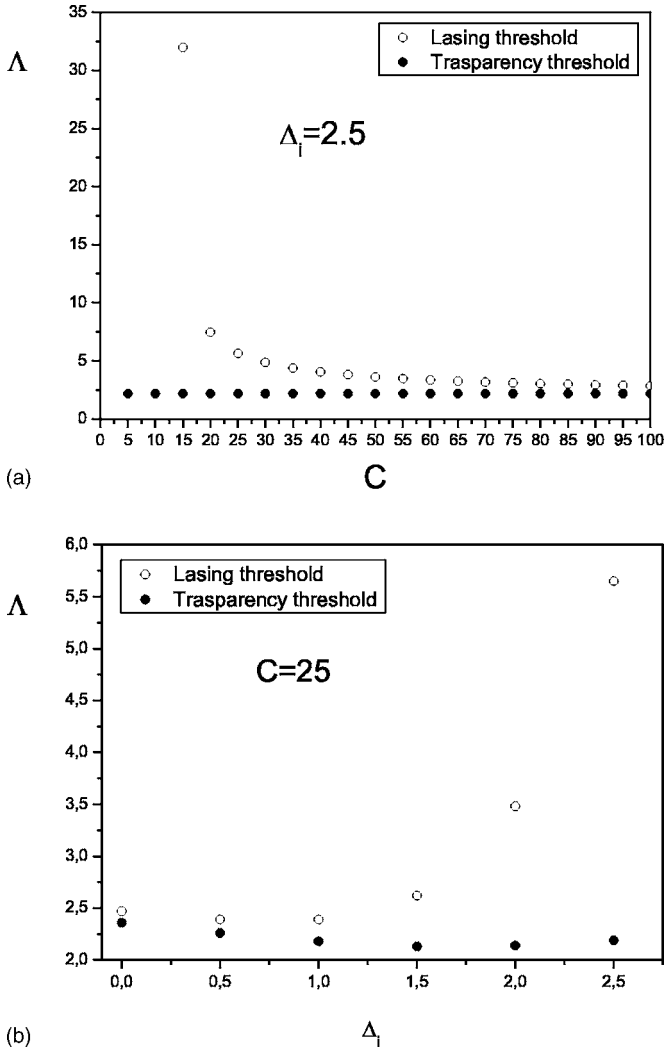

FIG. 3. Plot of the transparency threshold and lasing threshold vs C for $\Delta_i=2.5$ (a), and vs Δ_i for $C=25$ (b). Other parameters are $\beta=0.02$, $\bar{\sigma}_{\mathrm{cap}}=500$, $B_{he,eh}=500$, $\bar{\gamma}^e_{\mathrm{esc}}=0.01$, $\bar{\gamma}^h_{\mathrm{esc}}=100$, $\Gamma_{\mathrm{sp}}=2.5$, $D=0.41$, and $\theta=-2$.

the carrier density. Since the refractive index is related to the real part of the susceptibility and the gain is linked to its imaginary part, the alpha factor can be evaluated as

$$\alpha \propto \frac{\frac{\partial}{\partial N}\mathrm{Re}(\chi)}{\frac{\partial}{\partial N}\mathrm{Im}(\chi)} = \frac{\frac{\partial}{\partial N}\left[-\int \frac{\Delta}{1+\Delta^2}(n^e + n^h - 2)G(\Delta_i,\Delta)d\Delta\right]}{\frac{\partial}{\partial N}\left[-\int \frac{1}{1+\Delta^2}(n^e + n^h - 2)G(\Delta_i,\Delta)d\Delta\right]}, \tag{17}$$

where $N=\int(n_e+n_h)G(\Delta)d\Delta$ is the total density of electrons and holes.

We choose here to describe the alpha factor by its fundamental definition rather than introducing it phenomenologically via a linearization of the medium gain because, as recalled in the Introduction, the pumping occurs in the WL and we wish here to focus on the combined role of inhomo-

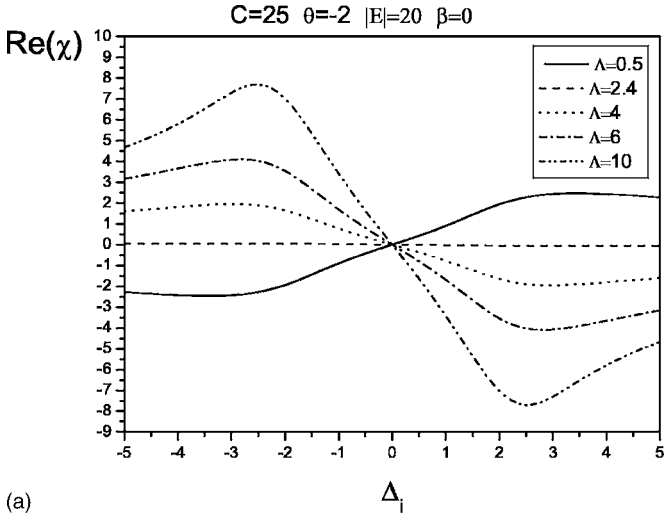

FIG. 4. Plot of the real (a) and imaginary (b) part of the susceptibility vs detuning from the QD population line center for five different values of the pump and for $\beta=0$ and $C=25$. Other parameters are as in Fig. 3.

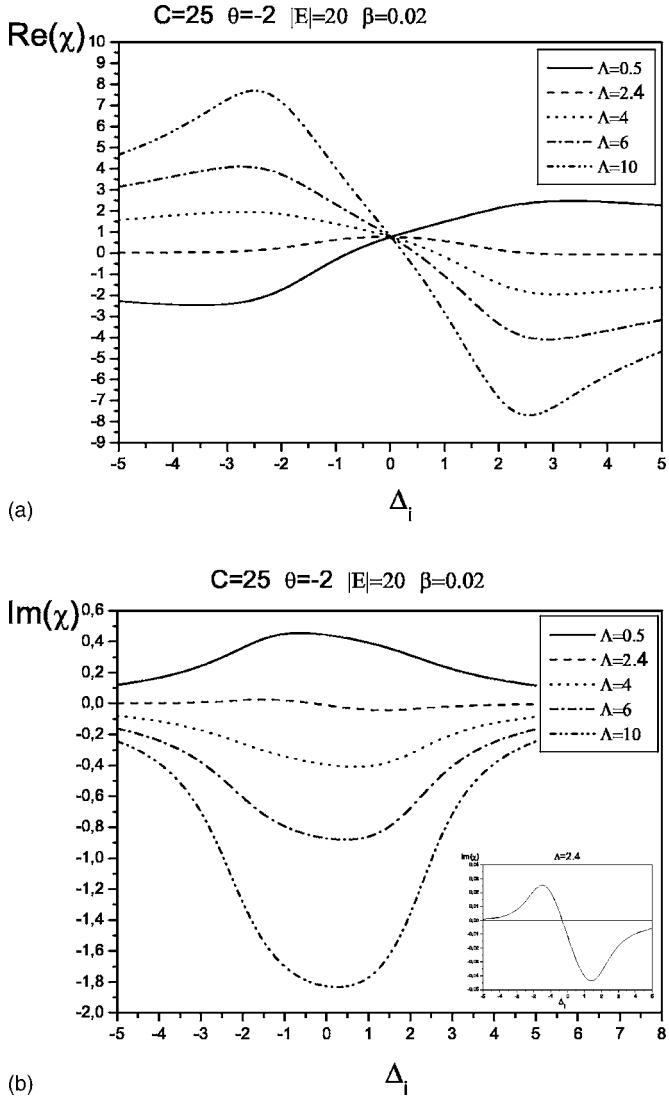

FIG. 5. Plot of the real (a) and imaginary (b) part of the susceptibility vs detuning from the QD population line center for five different values of the pump and for $\beta=0.02$. Other parameters are as in Fig. 4.

geneous broadening and QD-WL interactions, which already proved relevant for the system behavior in terms of modulational instabilities and pattern formation.

The spectral and carrier density dependencies of the real and imaginary part of the susceptibility are studied at a fixed intracavity field. The spectral density is obtained via a variation of the detuning parameter Δ_i, while a pump variation corresponds to a variation of the carrier density provided that other parameters are kept fixed. Figures 4(a) and 4(b) show the real part and the imaginary part, respectively, of the susceptibility versus energy for four different values of pump below and above transparency and for $\beta=0$. These graphs are proportional to the carrier-induced refractive index change and to the gain spectra, and they are symmetrical with respect to the injected frequency. Thus the behavior resembles the typical one of a two-level atom. Figure 4(a) depicts a crossing of the different curves, i.e., $d[\mathrm{Re}(\chi)]/dN=0$, at resonance with the injected field. Figure 4(b), on the other hand, shows the absorption/gain maximum is at resonance with the injected field, hence we recover the result that, in the absence of any asymmetry factor, when operating at peak gain, there is no linewidth broadening.[20]

When we introduce $\beta\neq 0$, the picture changes showing that a nonvanishing value of β directly affects the previously observed symmetry of the curves. In particular, the gain curve [Fig. 5(b)] is not symmetric anymore around the central frequency, and upon inspection of Fig. 5(a) we can conclude that the linewidth enhancement factor does not vanish at gain peak. $\Delta_i<0$ means that we are dealing mostly with higher-energy QD for which capture, as well as escape, is easier. On the whole, with our parameters, it seems that escape is the dominant mechanism so there is less gain than in the symmetric case. The same argument, reversed, explains why there is a higher gain for $\Delta_i>0$. In the following paragraphs, we will consider in finer detail such mechanisms acting on the populations providing the medium response.

In the presence of an asymmetry due to the dependence from Δ and Δ_i in the capture and escape rates, we expect a variation and a deviation of the peak gain as results in Fig. 5(b).

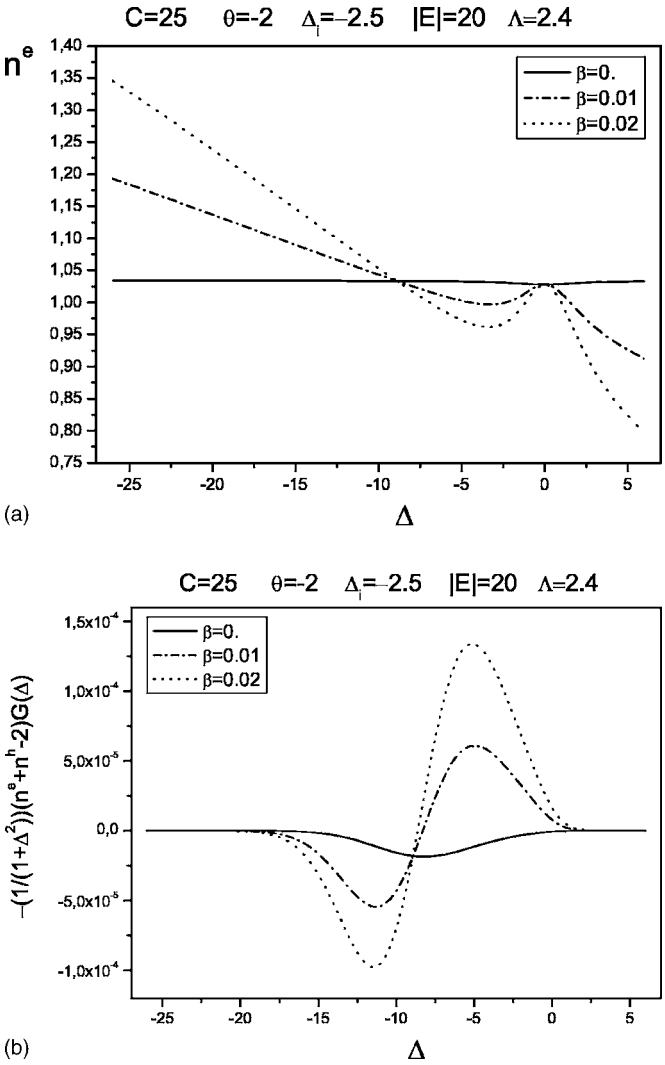

FIG. 6. (a) Electron-hole number distribution and (b) $-(1+\Delta^2)^{-1}(n^e+n^h-2)G(\Delta)$ for $\Delta_i=-2.5$, plotted for different values of β. $C=25$, $\vartheta=-2$, $|E_{\text{in}}|=20$, and $\Lambda=2.4$ Other parameters are as in Fig. 3.

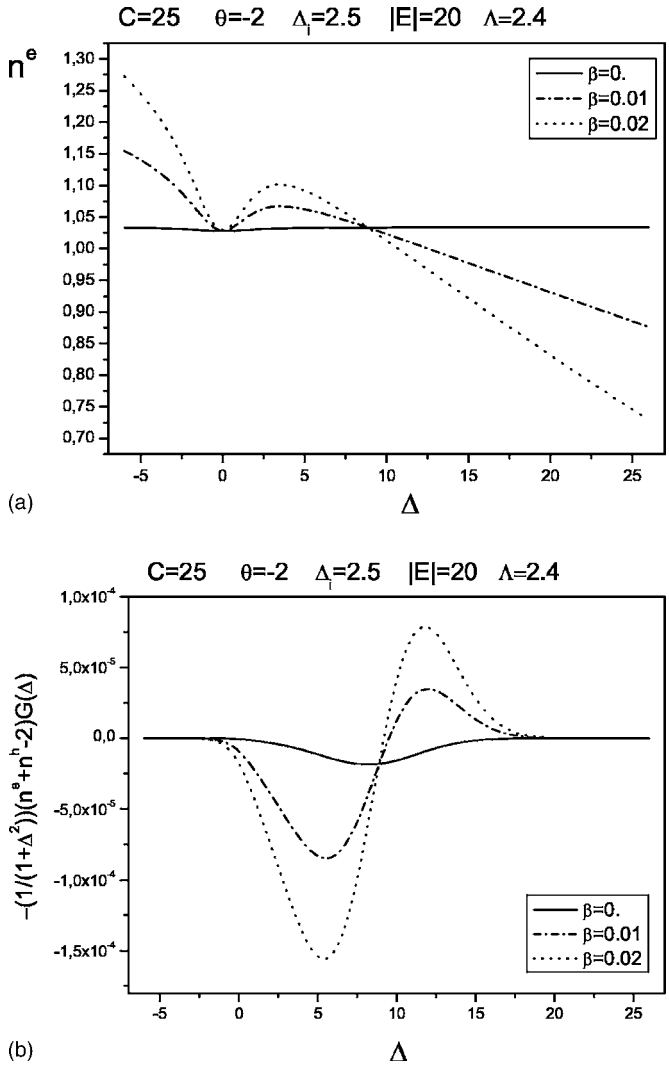

FIG. 7. The same as Fig. 6 here plotted for $\Delta_i=2.5$.

Asymmetrical carrier occupation is found because deeper QD contain more carriers, as would be expected by Fermi-Dirac statistics, which result from the equilibrium of the carriers within their bands.[20] By increasing the current supply, both the ground state and the excited state of the QD are almost fully populated as carriers begin to fill the WL. The asymmetric band filling of the broadened QD ground state is reflected as a redshift of peak gain in energy that ceases to change with further increase of the current density. In Fig. 5(a), as a general trend the crossover of $\delta n=0$corresponds to the peak of the gain spectra in Fig. 5(b), and the increase in carriers with an increment in the current density sees a larger variation of δn across the frequency range. This kind of behavior that is the variation and deviation of the peak gain can be observed also in Refs. 20 and 26.

In order to better interpret the behavior of the real and imaginary part of the susceptivity, it is instructive to analyze the distribution of the electron and hole occupation number n^e and n^h and also of the term $f(\Delta)=-(1+\Delta^2)^{-1}(n^e+n^h-2)G(\Delta)$ appearing as the integrand function in the susceptivity for different values of Δ_i versus Δ. In Fig. 6, we plot n^e and $f(\Delta)$ for $\Delta_i=-2.5$ and for different values of β, while in Fig. 7 the same quantities are considered for $\Delta_i=2.5$. For the sake of compactness, we do not report the plots of the hole occupation number since they are similar to those of electrons.

We now recall that gain corresponds to a negative imaginary part of the susceptivity that can be written as $\text{Im}(\chi)=\int f(\Delta)d\Delta$. By inspecting Figs. 6(b) and 7(b), we easily infer, looking at the total area under the curve, that when $\Delta_i<0$, the system absorbs, while when $\Delta_i>0$ there is gain. This justifies the behavior found in Fig. 5(b).

We want to stress that here n^e and n^h are occupation numbers, with transparency condition $n^e+n^h>2$, and so the physical distributions of electrons and holes are obtained by considering the integral of n^e and n^h weighted by the inhomogeneous broadening.

When beta is equal to zero, the carrier distribution is uniform versus Δ for any Δ_i at this value of the pump slightly above threshold [see, e.g., the horizontal black line in Figs. 6(a) and 7(a)]. When beta is different from zero, the carrier distribution is no longer uniform with respect to Δ and its negative slope versus Δ can be interpreted as follows.

The larger the difference in energy between WL and the ES, the longer the carriers will last in the excited state, i.e., it is more difficult for them to escape into the WL. The energy of the WL is a fixed parameter of the material under consideration, and so we note that when the energy of the exciton is high, the difference in energy with the WL becomes smaller, so the escape of the carrier is favored and hence we have less carrier. The opposite happens for lower exciton energies. The energy of the exciton can be cast as $\hbar\omega_a=\hbar\gamma\Delta+\hbar\omega_0$, where we see that the exciton energy depends on Δ via a direct proportionality. From the considerations written so far, we immediately see that high values of Δ favor carrier escape (we have less carrier) while low values of Δ inhibit carrier escape (we have more carriers).

Figures 6(a) and 7(a) show two features that merit some considerations: in Fig. 6(a), we note the presence of a small localized maximum for the region with less carrier, while in Fig. 7(a), we note the presence of a small local minimum in the region with more carriers, but more importantly, in both cases the localized maximum or minimum occurs for $\Delta=0$, which simply means that among all the various classes, we are considering the particular QD family that is resonant with the injected field. The width of this spectral hole burning becomes increasingly dominant as signal intensity increases, as is observed in Ref. 20. This behavior can be explained in the following manner. At resonance we have the maximum energy transfer among the QD class and the input field. If the resonance occurs in the low carrier region, where the system is below transparency, the injected field is absorbed and the absorbed energy promotes more carriers in the excited state (i.e., we note a local maximum for carriers). If the resonance occurs on the high carrier region, where the system is above transparency, the input field is amplified i.e., it absorbs energy from the carriers that in turn leave the excited state (i.e., we note a local minimum for carriers). This behavior is thus linked to the QD class, which is resonant with the injected field, and we should expect that the width of the local maximum (or of the local minimum) should be of the same order of the width of the single QD class. The width of the single QD class is 2γ; Δ is scaled with respect to γ itself, and so in units of Δ the width should be 2. The inspection of Figs. 6(a) and 7(a) does not confirm this, especially when for $\beta=0.02$ the width turns out to be about 4. This means that also spectral classes near the particular QD family that is resonant with the injected field are contributing to be absorbed or amplified.

The alpha factor $\alpha \propto (dn/dN)/(dg/dN)$ can then be numerically evaluated from the spectral dependence of the susceptivity simulated for different values of the pump. A QD material, having a symmetric gain profile, is theoretically predicted to have small $\partial(\delta n)/\partial N$ at each resonant state,[22] which results in $\alpha \approx 0$. As this property is broken by the inhomogeneity in dot size, the system is susceptible to carrier-density-dependent effects such as the band-filling effect[21] and the many-body effects,[26] which result in frequency-dependent peak gain, and δn characteristics that lead to α, which are sensitive to a change in carrier density. Figure 8 shows the α factor referring to the parametric case $C=25$, $\theta=-2$, $\beta=0.02$ and three different values of the pump. We observe the peculiar behavior of the alpha factor that becomes negative for energy injection above QD population line-center energy, that is to say, we see the trend of decreasing α with an increase in spectral energy. This is anomalous with respect to the usual behavior found for bulk medium, and it is due to a decreasing refractive index change with increasing carrier density.[27] This is observed also in Refs. 20 and 28.

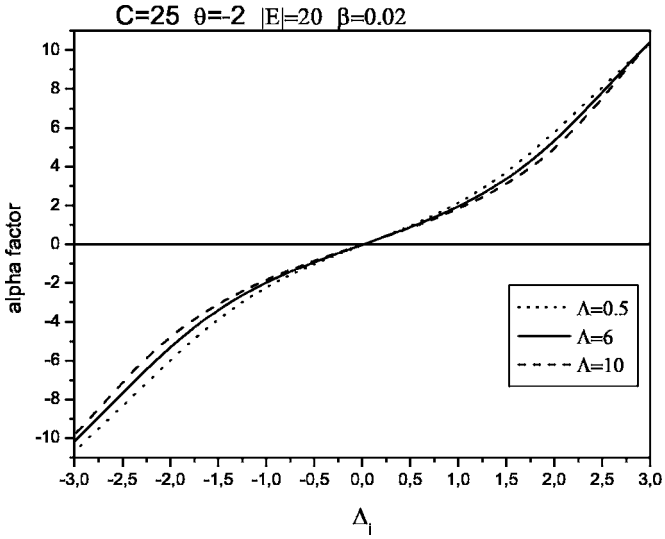

FIG. 8. Alpha factor for $C=25$, $\theta=-2$, and different value of the pump. Other parameters are as in Fig. 3.

The alpha factor can also be evaluated versus variation of the pumping term Λ. We report (see, e.g., Fig. 9) the calculated alpha factor versus Λ for the case $\Delta_i=2.5$ and -2.5. We note that due to the sign change in the real part of the susceptivity, the alpha factor simply changes sign for $\Delta_i=2.5$ and -2.5.

C. Analysis of steady-state curves and pattern

After having analyzed the optical response of the QD model especially for the alpha factor, we next studied the steady-state regimes with the aim of finding favorable conditions for the formation of patterns and cavity solitons. We scanned preliminarily the parameter domains in order to find a set for which the steady-state curve could follow some general criteria for which we expect a significantly broad range for stable localized structures. The guiding criteria for choosing a parametric set that is more suitable for investigation of cavity solitons can be summarized as follows:

(i) The curve should correspond to a bistable regime (S-shaped stationary curve).
(ii) The unstable portion of the high-intensity branch should be as extended as possible and at least a part of it should not coexist with the lower homogeneous branch.
(iii) The low-intensity homogeneous branch, ideally the whole of it, should be stable.

In this model, the linear stability analysis cannot be obtained algebraically and thus a simple expression for the Tur-

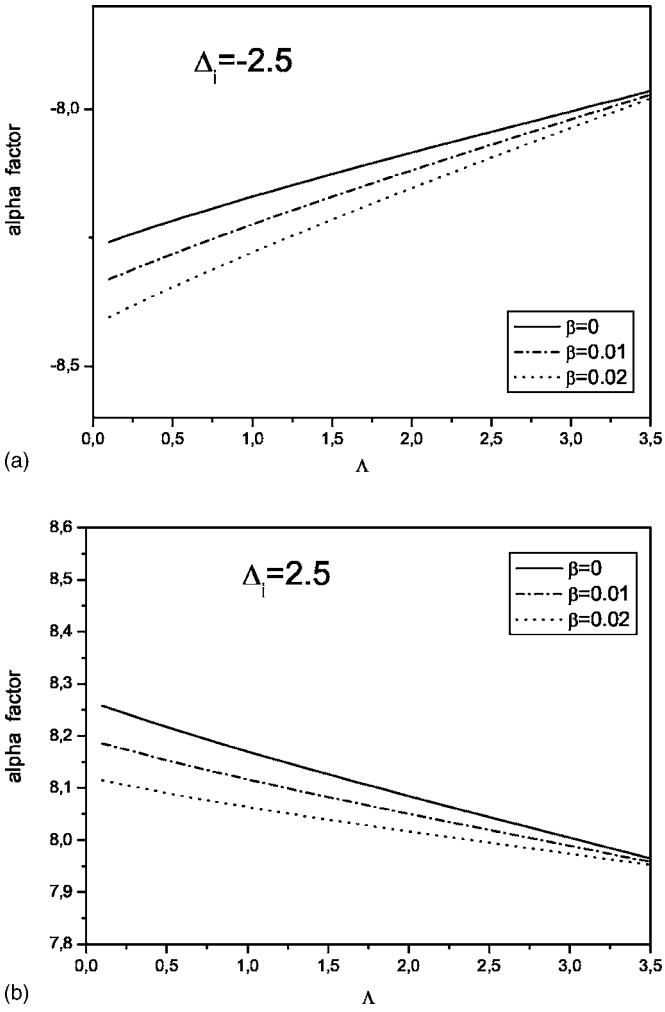

FIG. 9. Example of alpha factor variation vs pump for energy injection above (a) and below (b) QD population central line.

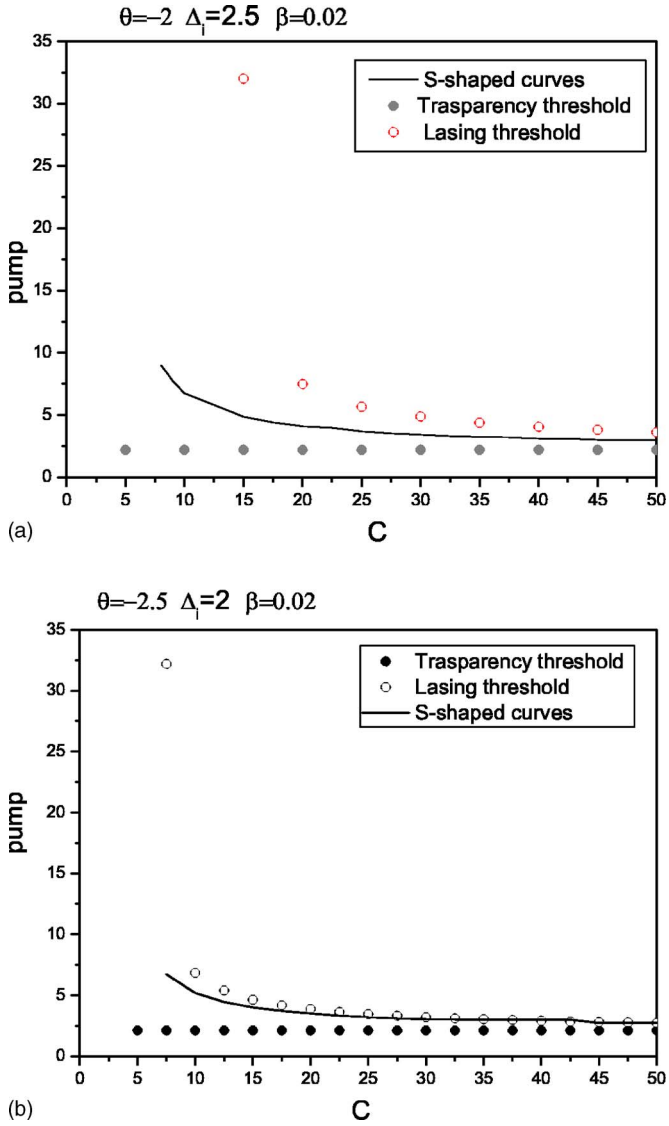

FIG. 10. (Color online) Investigation of S-shaped curves changing the values of the pump Λ and the bistable parameter C, for $\theta=-2$, $\Delta_i=2.5$, and $\beta=0.02$ (a) and for $\theta=-2.5$, $\Delta_i=2$, and $\beta=0.02$ (b). Other parameters are as in Fig. 3.

ing instability boundaries cannot be derived. An analysis of the homogeneous steady state can be performed in a numerical way. We searched for S-shaped curves looking for the turning points (if existent) of the steady-state homogeneous curve. Systematic studies were performed in the parameter space changing the values of two parameters at a time, for example the pump Λ and bistable parameter C, and then changing the cavity detuning θ or the detuning Δ_i. We realized that in order to have an alpha factor of a value around 5 or 6, we have to use a detuning, Δ_i, of about 2 or 2.5. So we decided to analyze the S-shaped curves for $\Delta_i=2$ and 2.5 and for small reasonable values of the coupling parameter C. Examples of these types of investigation are shown in Fig. 10. Here we have reported the pump values of the transparency threshold and of the laser threshold against C; in the same graph, we have also reported the curve of the pump values that give rise to a bistable steady-state homogeneous curve. This kind of systematic spanning of the parameter space is time-consuming and the whole scenario is also complicated by the fact that it may happen that some S-shaped curves do not exhibit the usual modulational instability of the upper branch. The range of the values of the pump and of the bistable parameter C has been changed for the different cases, obtaining graphs similar to the ones in Fig. 10. For the particular choice of parameters in Fig. 10, a bistability can be found significantly below the lasing threshold.

A possible parametric set for the realization of pattern and cavity solitons that we studied are thus as follows:

$\bar{\sigma}_{\mathrm{cap}}=500$, $B_{he,eh}=500$, $\bar{\gamma}^{e}_{\mathrm{esc}}=0.01$, $\bar{\gamma}^{h}_{\mathrm{esc}}=100$, $\Gamma_{\mathrm{sp}}=2.5$, $D=0.41$, $\beta=0.02$, $C=25$, $\theta=-2$, $\Delta_i=2.5$, and $\Lambda=4$, which is about 30% under threshold, and $C=10$, $\theta=-2.5$, $\Delta_i=2$, and $\Lambda=6.1$, which is about 10% under threshold.

The first check was to find the lasing threshold that is $\Lambda_{\mathrm{lasing}}=5.65$ for the first parametric set and $\Lambda_{\mathrm{lasing}}=6.85$ for the second set. The choice $\beta=0.02$ was determined by the fact that when fixing β different from zero, the bistable behavior is more evident, that is to say, the inclusion of the asymmetry factor in the gain profile, i.e., in the susceptivity, permits us to find favorable conditions for patterns and cavity solitons.

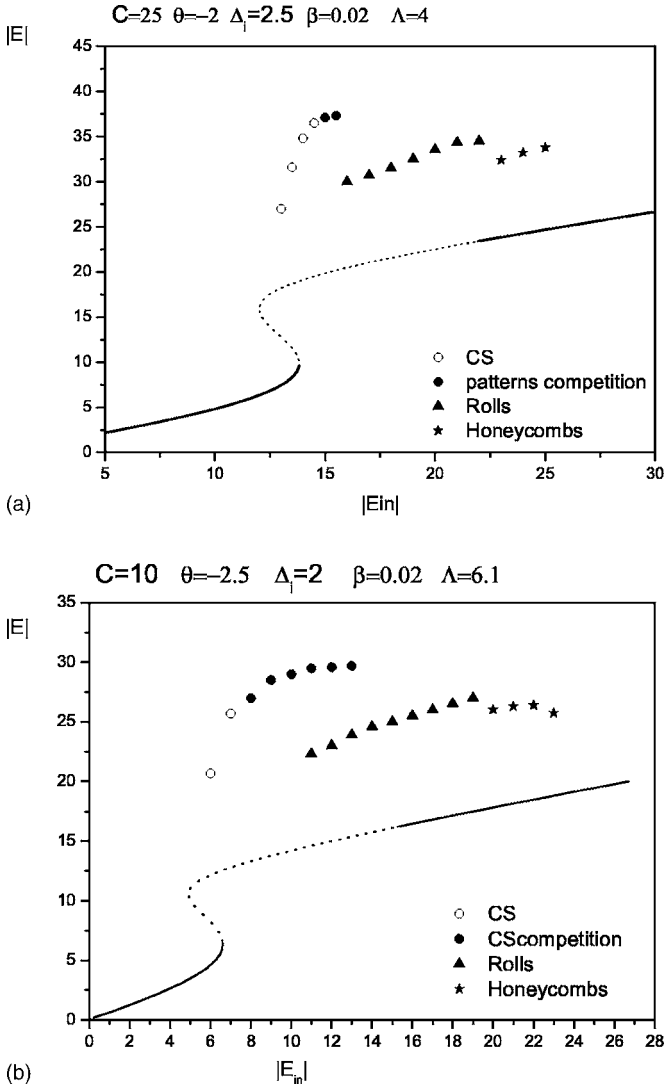

FIG. 11. Bistable S-shaped homogeneous curve and pattern and CS characterization for the case $\theta=-2$, $\Delta_i=2.5$, $C=25$, $\beta=0.02$, and $\Lambda=4$ (a) and $\theta=-2.5$, $\Delta_i=2$, $C=10$, $\beta=0.02$ and $\Lambda=6.1$ (b). The dotted portion of the S-shaped curve is unstable. Other parameters are as in Fig. 3.

Since the linear stability analysis cannot be performed algebraically, the analysis of the instabilities was done numerically.

In Figs. 11(a) and 11(b), we report the bistability curves with a characterization of patterns arising as self-organized structures and of CSs for the chosen parametric sets.

In the first case, stable CS are found in a range from $|E_{\text{in}}|=13$ to $|E_{\text{in}}|=14.5$; this is due to a general feature of CS, i.e., they need a stable lower branch on which to stand. By decreasing the input field amplitude down to 12.5, the system precipitates on the lower homogeneous branch, while by increasing the input field amplitude, the CS destabilize in favor of a competition between cavity solitons and rolls for $|E_{\text{in}}|=15$ and 15.5; then this pattern destabilizes in favor of roll patterns. They exist for a range of the input field amplitude, from $|E_{\text{in}}|=16$ to $|E_{\text{in}}|=22$, and then evolve to honeycomb patterns. Honeycomb patterns are met beyond the onset of the MI on the upper branch of the homogeneous curve; they exist for values of the input field amplitude in the range 23–25. The patterns observed are qualitatively comparable with those predicted in other nonlinear resonators, and their general scheme of evolution and competition is similar to previous studies.[13,29,30]

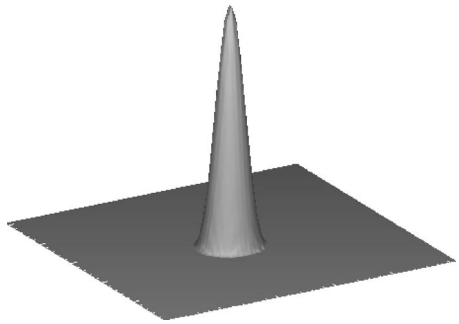

FIG. 12. CS profile sitting on the homogeneous background.

In the second case, the scenario is quite similar. Stable CS are found in a range from $|E_{\text{in}}|=6$ to $|E_{\text{in}}|=7$; this is due to the general feature of CS, i.e., they need a stable lower branch on which to stand. By decreasing the input field amplitude down to 5, the system precipitates on the lower homogeneous branch, while by increasing the input field amplitude, the CS destabilize in favor of a competition between cavity solitons and hexagons in a range from $|E_{\text{in}}|=8$ to $|E_{\text{in}}|=13$. These are not stable CS, but they endlessly move in the transverse plane as multiple ensembles of CS. Then this pattern destabilizes in favor of roll patterns. They exist for a range of the input field amplitude, from $|E_{\text{in}}|=11$ to $|E_{\text{in}}|=19$, and then evolve to honeycomb patterns. Honeycomb patterns exist for values of the input field amplitude in the range 20–23.

We have also observed that everywhere the spontaneously organized CS are stable; we could also independently address and switch on/off CS by means of narrow Gaussian pulses, superimposed to the homogeneous background, centered at the point at which we want to create or annihilate the CS. In Fig. 12, we show a CS at a regime sitting on the homogeneous background.

Summing up both of the cases analyzed might in principle be adopted for an experimental search for CS in such systems.

V. CONCLUSION

In this paper, we have developed an extended model for the description of the optical response of a QD semiconductor microcavity both in the absorbing and amplifying regime. We have traced the way that we have adopted for subsequent refinements of the model starting from the simple two-level inhomogeneously broadened description up to the inclusion for the QD-WL interactions. The role of the various interaction mechanisms has been investigated in connection with the optical regimes under consideration. A key point in the modelization has been the inclusion of QD transition energies and single dot detuning dependence in the escape and capture terms, which in turn are responsible for a gain asymmetry in the active configuration.

We have reviewed the results already obtained in the passive configuration, and we have checked that the energy dependencies of the escape and capture terms do not alter the favorable scenario for pattern-forming instabilities and CS formation especially in the focusing regime, which is by far the most relevant regime for an experimental search of CS.

As for the active regime, here investigated for the first time, we have first analyzed the response of the system in terms of the alpha enhancement factor and we have analyzed the important role played by the gain asymmetries. We have then performed a detailed analysis of the parameter space in order to find the best suitable regime for CS and global structure formation. Special attention has been devoted to the numerical values of the bistability parameter C since it is directly related to the QD density; thus a lower value of C would be preferable from an experimental point of view. The first numerical investigations are encouraging in this sense since we have found reliable parameter ranges down to $C=10$.

The next step of our study will be a closer comparison of all the numerical parameters adopted in the model with the experimental indications coming out from the experiments in due course at LPN.

ACKNOWLEDGMENTS

The authors acknowledge partial support from the European Commission through the STREP project No. 004868 (FunFACS).

[1]M. Brambilla, L. A. Lugiato, F. Prati, L. Spinelli, and W. J. Firth, Phys. Rev. Lett. **79**, 2042 (1997).
[2]S. Barland, J. R. Tredicce, M. Brambilla, L. A. Lugiato, S. Balle, M. Giudici, T. Maggipinto, L. Spinelli, G. Tissoni, T. Knödel, M. Miller, and R. Jäager, Nature **419**, 699 (2002).
[3]X. Hachair, L. Furfaro, J. Javaloyes, M. Giudici, S. Balle, J. Tredicce, G. Tissoni, L. A. Lugiato, M. Brambilla, and T. Maggipinto, Phys. Rev. A **72**, 013815 (2005).
[4]Y. Menesguen, S. Barbay, X. Hachair, L. Leroy, I. Sagnes, and R. Kuszelewicz, Phys. Rev. A **74**, 023818 (2006).
[5]S. Barbay, Y. Ménesguen, X. Hachair, L. Leroy, I. Sagnes, and R. Kuszelewicz, Opt. Lett. **31**, 1504 (2006).
[6]X. Hachair, F. Pedaci, E. Caboche, S. Barland, M. Giudici, J. R. Tredicce, F. Prati, G. Tissoni, R. Kheradmand, L. A. Lugiato, I. Protsenko, and M. Brambilla, IEEE J. Sel. Top. Quantum Electron. **12**, 339 (2006).
[7]M. Bache, F. Prati, G. Tissoni, R. Kheradmand, L. A. Lugiato, I. Protsenko, and M. Brambilla, Appl. Phys. B: Lasers Opt. **81**, 913 (2005).
[8]M. Grundmann, Physica E (Amsterdam) **5**, 167 (1999).
[9]G. Huyet, D. O'Brien, S. P. Hegarty, J. G. McInerney, A. V. Uskov, D. Bimberg, C. Ribbat, V. M. Ustinov, A. E. Zhukov, S. S. Mikhrin, A. R. Kovsh, J. K. White, and K. Hinzer, Phys. Status Solidi A **201**, 345 (2004).
[10]E. A. Viktorov, P. Mandel, I. O'Driscoll, O. Carroll, G. Huyet, J. Houlihan, and Y. Tanguy, Opt. Lett. **31**, 2302 (2006).
[11]M. Segev, B. Crosignani, A. Yariv, and B. Fischer, Phys. Rev. Lett. **68**, 923 (1992).
[12]N. Fressengeas, J. Maufoy, and G. Kugel, Phys. Rev. E **54**, 6866 (1996).
[13]L. Spinelli, G. Tissoni, M. Brambilla, F. Prati, and L. A. Lugiato, Phys. Rev. A **58**, 2542 (1998).
[14]M. Sugawara, H. Ebe, N. Hatori, M. Ishida, Y. Arakawa, T. Akiyama, K. Otsubo, and Y. Nakata, Phys. Rev. B **69**, 235332 (2004).
[15]C. Gies, J. Wiersig, M. Lorke, and F. Jahnke, Phys. Rev. A **75**, 013803 (2007).
[16]W. W. Chow and S. W. Koch, IEEE J. Quantum Electron. **41**, 495 (2005).
[17]J. Hader, J. V. Moloney, S. W. Koch, and W. W. Chow, IEEE J. Sel. Top. Quantum Electron. **9**, 688 (2003).
[18]S. Barbay, J. Koehler, R. Kuszelewicz, T. Maggipinto, I. M. Perrini, and M. Brambilla, IEEE J. Quantum Electron. **39**, 245 (2003).
[19]I. M. Perrini, S. Barbay, T. Maggipinto, M. Brambilla, and R. Kuszelewicz, Appl. Phys. B: Lasers Opt. **81**, 905 (2005).
[20]H. C. Wong, G. B. Ren, and J. M. Rorison, Opt. Quantum Electron. **38**, 395 (2006).
[21]J. Oksanen and J. Tulkki, J. Appl. Phys. **94**, 1983 (2003).
[22]S. Melnik, G. Huyet, and A. V. Uskov, Opt. Express **14**, 2950 (2006).
[23]A. Markus, J. X. Chen, O. Gauthier-Lafaye, J. G. Provost, C. Paranthoen, and A. Fiore, IEEE J. Sel. Top. Quantum Electron. **9**, 1308 (2003).
[24]E. A. Viktorov, P. Mandel, Y. Tanguy, J. Houlihan, and G. Huyet, Appl. Phys. Lett. **87**, 053113 (2005).
[25]M. Brambilla, L. A. Lugiato, F. Prati, L. Spinelli, and W. J. Firth, Phys. Rev. Lett. **79**, 2042 (1997).
[26]M. Gioannini, A. Sevega, and I. Montrosset, Opt. Quantum Electron. **38**, 381 (2006).
[27]H.C. Schneider, W.W. Chow, and S.W. Koch, Phys. Rev. B **66**, 041310(R) (2002).
[28]S. Schneider, P. Borri, W. Langbein, U. Woggon, R. L. Selling, D. Ouyang, and D. Bimberg, IEEE J. Quantum Electron. **40**, 1423 (2004).
[29]G. Tissoni, L. Spinelli, M. Brambilla, T. Maggipinto, I. Perrini, and L. A. Lugiato, J. Opt. Soc. Am. B **16**, 2083 (1999).
[30]G. Tissoni, L. Spinelli, M. Brambilla, T. Maggipinto, I. Perrini, and L. A. Lugiato, J. Opt. Soc. Am. B **16**, 2095 (1999).